First principles investigation of the electronic and structural properties of $Mg_{3x}Be_{3-3x}N_2$ ternary alloy

2004 J. Phys.: Condens. Matter 16 6063

(http://iopscience.iop.org/0953-8984/16/34/007)

INSTITUTE OF PHYSICS PUBLISHING JOURNAL OF PHYSICS: CONDENSED MATTER

J. Phys.: Condens. Matter **16** (2004) 6063–6074 PII: S0953-8984(04)80759-8

First principles investigation of the electronic and structural properties of $Mg_{3x}Be_{3-3x}N_2$ ternary alloy

A Mokhtari and H Akbarzadeh[1]

Department of Physics, Isfahan University of Technology, Isfahan 8415683111, Iran

E-mail: Akbarzad@cc.iut.ac.ir

Received 12 May 2004
Published 13 August 2004
Online at stacks.iop.org/JPhysCM/16/6063
doi:10.1088/0953-8984/16/34/007

Abstract

The first *ab initio* calculations were carried out for the electronic and structural properties of the wide band gap semiconductor alloy $Mg_{3x}Be_{3-3x}N_2$ employing the full potential linearized augmented plane wave (FP-LAPW) method within density functional theory (DFT). We used the Perdew *et al* generalized gradient approximation (GGA96), which is based on exchange–correlation energy optimization, to optimize the internal parameters by relaxing the atomic positions in the force directions and to calculate the total energy. For band structure calculations, we utilized both the Engel–Vosko's generalized gradient approximation (EVGGA), which optimizes the exchange–correlation potential, and also GGA96. We investigated the effect of composition on a variety of different structural and electronic parameters such as lattice constant, bond length, internal parameter, bulk modulus and band gap. We found out that the linear concentration dependence (LCD) is inadequate to explain the results, hence we fitted our data with a quadratic expression and were able to obtain the bowing parameter for each case. Our results for the band gap, lattice parameter, cohesive energy and bulk modulus indicate that each of them can be explained by a constant bowing parameter.

1. Introduction

Wide band gap semiconductors are currently under intense investigations due to their unusual properties as well as their possible applications in electronic and optoelectronic devices. By alloying them, it is possible to tune the wavelength of emitted light through a wide spectral region and it could offer the opportunity to create a new family of wide band gap semiconductor compounds. Among them nitrogen-based semiconductor compounds [1–8] and their alloys [1, 9–11] have attracted considerable interest in the last few years due to their applications in optoelectronic light emitting diodes, laser diodes operating in the green–blue

[1] Author to whom any correspondence should be addressed.

near UV region, high speed applications and high-density optical data storage, and also their having a high thermal conductivity and large bulk modulus.

Nitrides of the group II elements such as α-(Be, Ca)$_3$N$_2$ [3, 5–7] and Mg$_3$N$_2$ [3, 5, 7] are salt-like with the metal cation and nitride anion. Among them α-Be$_3$N$_2$ and Mg$_3$N$_2$ compounds are iso-structural and have direct band gaps (Γ–Γ) in the visible range with values of 4.17 and 2.22 eV respectively [3]. Therefore they are appropriate candidates for alloying. Our goal is to study the electronic and structural properties of the ternary alloy Mg$_{3x}$Be$_{3-3x}$N$_2$. To our knowledge no theoretical or experimental work has yet been reported on the electronic and structural properties of this alloy, therefore this study can be considered as the first *ab initio* investigation of this material.

In this paper we focus our attention on the variation of different structural and electronic parameters such as lattice constant, internal parameter, bulk modulus and band gap with composition. For all of these parameters we fitted our results with a quadratic expression which has been written below for the energy gap:

$$E_g(\mathrm{Mg}_{3x}\mathrm{Be}_{3-3x}\mathrm{N}_2) = xE_g(\mathrm{Mg}_3\mathrm{N}_2) + (1-x)E_g(\mathrm{Be}_3\mathrm{N}_2) - bx(1-x)$$

where the so-called bowing parameter b accounts for the deviation from a linear interpolation between the two binary Mg$_3$N$_2$ and Be$_3$N$_2$ compounds and we have neglected higher-order terms in the expansions. This definition is typically used to describe the non-linear behaviour of the band gap for alloys, while in this paper we have extended this definition to the other parameters too. The situation becomes more complicated if E_g or other parameters depend in a non-quadratic manner on x. In this case a concentration-dependent bowing function $b(x)$ can be defined. In many cases $b(x)$ approximately shows a linear dependence on concentration [9].

This paper is organized as follows. In section 2 we give a brief description of the computational method. Results and discussion concerning electronic and structural properties of Mg$_{3x}$Be$_{3-3x}$N$_2$ alloy are presented in sections 3 and 4 contains the conclusions.

2. Method of calculations

The calculations are performed using the scalar relativistic FP-LAPW approach as implemented in WIEN2K [12] code within the framework of density functional theory (DFT) [13, 14]. The exchange–correlation energy of electrons is described in generalized gradient approximation (GGA96) [15] to calculate the total energy and in Engel–Vosko's generalized gradient (EVGGA) [16] formalism, which optimizes the corresponding potential, for band structure calculations. In the FP-LAPW method, the wavefunction, charge density and potential are expanded by spherical harmonic functions inside non-overlapping spheres surrounding the atomic sites (muffin-tin spheres) and by a plane waves basis set in the remaining space of the unit cell (interstitial region). A mesh of $5\times5\times5$ special k-points is taken in the whole Brillouin zone. The maximum l quantum number for the wavefunction expansion inside atomic spheres is confined to $l_{\max} = 10$. The plane wave cutoff of $K_{\max} = 7.0/R_{\mathrm{MT}}$ (R_{MT} is the smallest muffin-tin radius in the unit cell) is chosen for the expansion of the wavefunctions in the interstitial region while the charge density is Fourier expanded up to $G_{\max} = 14$. Both the plane wave cutoff and the number of k-points are varied to ensure total energy convergence.

3. Results and discussion

3.1. Structural properties

The cubic phase of M$_3$N$_2$ (M = Be, Mg) has an anti-bixbyte structure in the body centred space group Ia_3 (206) [17] with 40 atoms per primitive cell, 24 similar M and two types of N atoms, 4N1 and 12N2. M atoms have three internal parameters (x, y, z) while N2 atoms

Table 1. Internal parameters obtained for the $Mg_{3x}Be_{3-3x}N_2$ structure at $x = \frac{1}{3}, \frac{2}{3}$.

X	u_2, u_3, u_4	x_1, y_1, z_1	x_2, y_2, z_2	x_3, y_3, z_3
1/3	0.0001, 0.0105, 0.9463	0.3909, 0.1269, 0.3852	0.3808, 0.1643, 0.3892	0.3898, 0.1521, 0.3616
2/3	0.9610, 0.9984, 0.9862	0.3890, 0.1436, 0.3702	0.3717, 0.1448, 0.4042	0.3884, 0.1709, 0.3893

have only one (u). The positions of N1 atoms are independent of any internal parameter. The values of x, y, z and u parameters were obtained by relaxing the atomic positions in the force direction and subsequently by lattice parameter optimization. Their dimensionless values for Be_3N_2 and Mg_3N_2 compounds were obtained as 0.385, 0.147, 0.381, 0.978 and 0.389, 0.153, 0.383, 0.969 respectively.

To model the $Mg_{3x}Be_{3-3x}N_2$ random alloy in general, the time consuming supercell approach is needed and different atomic configurations should be considered. In this system the unit cell is quite large and the smallest supercell, which corresponds to a $2 \times 2 \times 2$ supercell, has 320 atoms. Therefore quantum calculations for such supercells are very time consuming. Furthermore, for each composition it is practically impossible to treat all different atomic configurations. Therefore by considering the symmetry of the system we first classified the 24 positions of M atoms in M_3N_2 compound into three distinct groups for making an alloy with $x = \frac{1}{3}, \frac{2}{3}$ and four groups (completely independent of first classification) for $x = \frac{1}{4}, \frac{2}{4}, \frac{3}{4}$. Then for each composition we randomly substituted an appropriate group of Be atoms in Be_3N_2 structure by Mg elements. Such substitution decreases the number of symmetry operations from the original value of 24 to 8 or 6 depending on concentration. A special arrangement of the atomic positions for all compositions is given in the appendix and we briefly explain them here. For $x = \frac{1}{3}$ and $\frac{2}{3}$ the number of symmetry operators reduces to eight and we have four types of nitrogen, 4N1, 4N2, 4N3, 4N4, with three internal parameters (u_2, u_3 and u_4). In the case of $x = \frac{1}{3}$ we only have one group of magnesium atoms, 8Mg1, with three internal parameters (x_1, y_1 and z_1) and two kinds of beryllium atoms, 8Be2 and 8Be3, with six internal parameters (x_i, y_i, z_i; $i = 2, 3$) while for $x = \frac{2}{3}$ we have two groups of magnesium atoms, 8Mg1 and 8Mg2, with six internal parameters (x_i, y_i, z_i; $i = 1, 2$) and only one type of beryllium atoms, 8Be3, with three internal parameters (x_3, y_3 and z_3). In the case of $x = \frac{1}{4}, \frac{2}{4}, \frac{3}{4}$ the number of symmetry operators reduces to six and there are four types of nitrogen atoms, 1N1, 3N2, 6N3 and 6N4, with six internal parameters (v_i, v_i'; $i = 1, 2, 3$). For $x = \frac{1}{4}$ there is one group of Mg atoms, (6Mg1), with three internal parameters (x_1, y_1 and z_1) and three types of beryllium atoms, (6Be2, 6Be3, 6Be4) with totally nine internal parameters (x_i, y_i, z_i; $i = 2, 3, 4$). In the cases of $x = \frac{2}{4}$ and $\frac{3}{4}$ we substituted one group of beryllium atoms, 6Be2, with 6Mg2 and two groups (6Be2, 6Be3) with 6Mg2 and 6Mg3 atoms respectively.

As no calculated or experimental value for the internal parameters of this alloy has been reported in the literature, we first calculated their roughly optimized values for each concentration by relaxing the atomic positions in the force directions using the lattice parameters that are obtained from Vegard's law. Then we used the optimized internal parameters to calculate the total energy for several lattice volumes and by fitting the results with the Murnaghan equation of state [18], the equilibrium lattice parameter at each composition was calculated. Finally, using the new optimized lattice parameter, once again we recalculated more accurate values of the internal parameters. Our calculated results for the internal parameters are reported in tables 1 and 2. The calculated equilibrium lattice constants, cohesive energy

Table 2. Internal parameters obtained for the $Mg_{3x}Be_{3-3x}N_2$ structure at $x = \frac{1}{4}, \frac{2}{4}, \frac{3}{4}$.

X	v_1, v_2, v_3	v'_1, v'_2, v'_3	x_1, y_1, z_1	x_2, y_2, z_2	x_3, y_3, z_3	x_4, y_4, z_4
1/4	0.9590, 0.9900, 0.2397	0.0120, 0.5197, 0.2612	0.3978, 0.1483, 0.3917	0.3830, 0.1635, 0.3794	0.3826, 0.1427, 0.3725	0.3786, 0.1427, 0.3855
2/4	0.9696, 0.9885, 0.2314	0.0271, 0.4930, 0.2655	0.3966, 0.1605, 0.3836	0.3812, 0.1671, 0.3930	0.3683, 0.1634, 0.3908	0.3879, 0.1327, 0.3957
3/4	0.9712, 0.9981, 0.2211	0.0305, 0.5003, 0.2514	0.3693, 0.1616, 0.4054	0.3732, 0.1849, 0.3924	0.3629, 0.1650, 0.3927	0.3999, 0.1248, 0.4040

Table 3. Lattice parameters, bulk modulus (B), its pressure derivative (B') and cohesive energy per atom obtained within GGA96 for $Mg_{3x}Be_{3-3x}N_2$ ternary alloy.

X		Lattice parameter a (Å)	B (Mbar)	B'	E_{coh} (eV/atom)
0	Our previous work[a]	8.156	2.168	3.60	6.633
	Calc.[b]	8.155	2.57	2.93	—
	Calc.[c]	8.144	2.52	2.71	6.626
	Exp.[d]	8.145	—	—	—
1/4	Our work	8.712	1.773	4.23	6.077
1/3	Our work	8.885	1.654	4.40	5.874
2/4	Our work	9.275	1.424	3.75	5.568
2/3	Our work	9.621	1.284	4.77	5.271
3/4	Our work	9.728	1.220	3.60	5.180
1	Our previous work[a]	10.037	1.110	4.02	4.979
	Calc.[b]	9.858	1.65	3.66	—
	Exp.[d]	9.96	—	—	—

[a] Reference [3].
[b] Reference [5].
[c] Reference [6].
[d] Reference [17].

per primitive cell, bulk modulus and its pressure derivative for all compositions are presented in table 3. The interatomic distances calculated using the optimized internal parameters and equilibrium lattice constants, are reported in table 4 and the composition dependence of the mean bond length for Mg–N and Be–N are shown in figure 1. An upward bowing, figure 2, with bowing parameter equal to -0.704 Å, is obtained for the lattice parameters by fitting the calculated values with a polynomial function. In figure 3, the composition dependence of the bulk modulus is compared with the results predicted by linear concentration dependence (LCD). A large deviation from LCD, with downward bowing equal to 0.802 Mbar, is clearly visible. The higher compressibility of the alloy compared to the values predicted by linear interpolation of the bulk modulus seems to be due to the fact that atoms in an alloy occupy less symmetric sites than in a pure compound and therefore have more freedom to relax and lower the total energy. The main features to note from the above calculations are as follows:

(1) The 10% mismatch between the lattice parameters of α-Be_3N_2 and Mg_3N_2 binary compounds as a possible source of lattice parameter bowing is not completely ruled

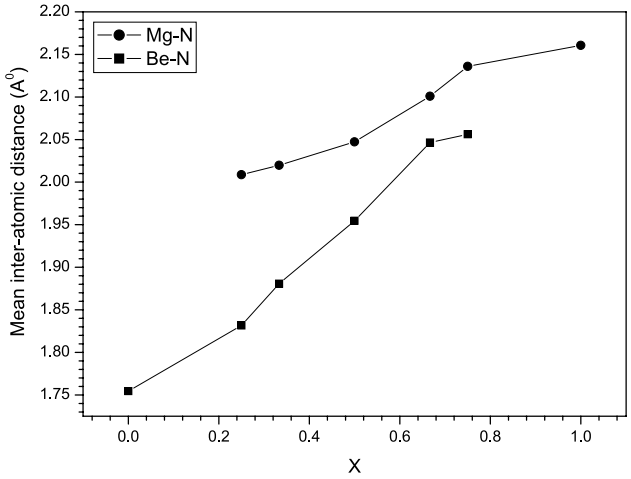

Figure 1. Composition dependence of the calculated average bond length in $Mg_{3x}Be_{3-3x}N_2$ alloy.

Table 4. Calculated bond lengths (Å) using optimized internal parameters and equilibrium lattice constant.

X	Å			
	M–N1	M–N2		
0	1.755	1.702, 1.770, 1.791		
1	2.160	2.101, 2.182, 2.199		
1/3	Mg1–(N1, N2, N3, N4)	Be2–(N1, N2, N3, N4)	Be3–(N1, N2, N3, N4)	
	2.051, 1.912, 2.025, 2.092	1.860, 1.634, 2.234, 1.812	1.812, 2.209, 1.734, 1.750	
2/3	Mg1–(N1, N2, N3, N4)	Mg2–(N1, N2, N3, N4)	Be3–(N1, N2, N3, N4)	
	2.042, 1.932, 2.286, 2.022	2.144, 2.056, 2.372, 1.951	2.037, 2.126, 1.702, 2.321	
1/4	Mg1–(N1, N3, N4, N4)	Be2–(N2, N3, N4, N4)	Be3–(N2, N3, N4, N4)	Be4–(N2, N3, N3, N3)
	1.992, 1.897, 2.018, 2.129	1.784, 1.998, 1.667, 1.862	1.830, 1.766, 1.898, 1.936	1.877, 1.636, 1.857, 1.869
2/4	Mg1–(N1, N3, N4, N4)	Mg2–(N2, N3, N4, N4)	Be3–(N2, N3, N4, N4)	Be4–(N2, N3, N3, N3)
	2.018, 1.999, 2.010, 2.107	1.958, 2.178, 1.934, 2.174	1.885, 2.248, 1.836, 2.073	2.155, 1.692, 1.808, 1.937
3/4	Mg1–(N1, N3, N4, N4)	Mg2–(N2, N3, N4, N4)	Mg3–(N2, N3, N4, N4)	Be4–(N2, N3, N3, N3)
	2.078, 2.087, 1.935, 2.388	1.925, 2.359, 1.922, 2.433	1.941, 2.520, 1.996, 2.047	2.512, 1.852, 1.900, 1.959

out [10, 19], although we have to notice that Vegard's law is obeyed by some other compounds even with strong lattice mismatch.

(2) Taking into consideration the results shown in figures 1 and 3, it can be concluded that the smaller average bond length the larger the bulk modulus, consistent with the semi-empirical Cohen's equation [20].

(3) In all compositions, the Mg–N bond is longer than Be–N. This behaviour is consistent with Pauling's empirical rule that the cation–anion distance is determined by the radius sums. It may also be due to the fact that the electronegativity of the Mg (1.2) atom is smaller than the Be (1.5), so that the Mg–N bond is more ionic and less rigid than the Be–N bond [21].

(4) The cohesive energy is defined as the difference between the total energy of isolated atoms and the corresponding crystal energy per primitive cell. In order to obtain an accurate value for the cohesive energy, the energy calculations for both the isolated atoms and the

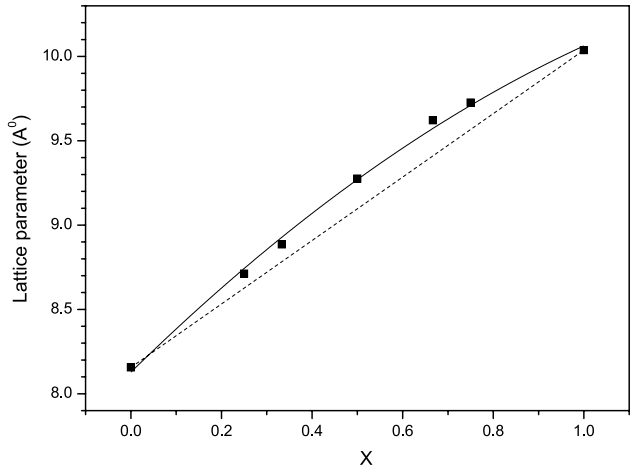

Figure 2. Composition dependence of the calculated lattice constant of cubic $Mg_{3x}Be_{3-3x}N_2$ ternary alloy (solid squares) compared with Vegard's prediction (dashed line). A bowing parameter equal to -0.704 Å is obtained by fitting the calculated values with a polynomial function (solid curve).

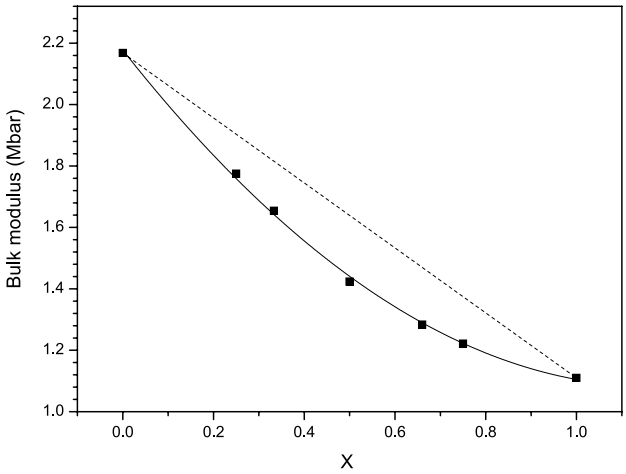

Figure 3. Composition dependence of the calculated bulk modulus of $Mg_{3x}Be_{3-3x}N_2$ alloy (solid squares) compared with the LCD prediction (dashed line). The bowing parameter equal to 0.802 Mbar was obtained by polynomial fitting (solid curve).

crystal need to be performed at the same level of accuracy. To fulfill such a requirement the energy of each isolated atom was calculated by considering a large cell containing one isolated atom. The size of this cell was chosen so large that the energy convergence was less than 0.001 Ryd. (A large cubic cell with dimension of 19 au for N and 17 au for Mg and Be atoms was needed for this convergence.) In this approach the relativistic effects are considered at the same level (scalar relativistic) for both the isolated atoms and crystal energy calculations. Hence the calculated cohesive energy in this method is reliable. The calculated cohesive energy shows a downward bowing from linear interpolation between end points, as is seen in figure 4. The value of the bowing parameter for cohesive energy is 0.9966 eV/atom.

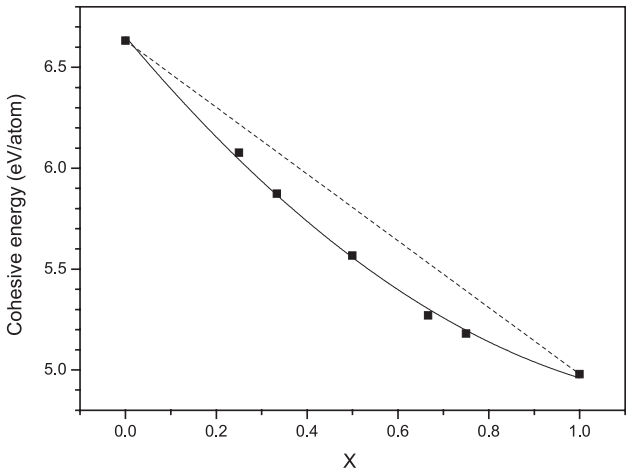

Figure 4. Composition dependence of the calculated cohesive energy of $Mg_{3x}Be_{3-3x}N_2$ alloy (solid squares) compared with the LCD prediction (dashed line). The bowing parameter equal to 0.9966 eV/atom was obtained by polynomial fitting (solid curve).

The formation energy of the alloy is defined as $\Delta E_x = E_{Mg_{3x}Be_{3-3x}N_2} - xE_{Mg_3N_2} - (1-x)E_{Be_3N_2}$, where $E_{Mg_{3x}Be_{3-3x}N_2}$, $E_{Mg_3N_2}$, and $E_{Be_3N_2}$ are the respective energies for $Mg_{3x}Be_{3-3x}N_2$ alloy, and Mg_3N_2 and Be_3N_2 compounds. By using the data displayed in figure 4 it is clearly seen that the formation energy of this alloy for all concentrations is positive. A similar behaviour is predicted for disordered semiconductor alloys [22]. This means that the alloy is thermodynamically unstable while it can be formed as a solid solution in metastable phase.

3.2. Band structure and density of state

The main shortcoming of density functional theory is rooted in the exchange–correlation term that cannot be handled accurately in this method. As a result of this deficiency, the energy gap is usually underestimated in this approach. Although in most solids advanced GGAs can improve the results compared to LDA, none of them are able to simultaneously obtain the exchange–correlation energy and its charge derivative accurately. This is due to the fact that GGA in general has a simple functional form that is not sufficiently flexible to accurately reproduce both of them. Engel and Vosko [16], by considering this shortcoming, constructed a new functional form of exchange–correlation potential (EVGGA) and were able to better reproduce the exchange potential at the expense of less agreement in exchange energy. The EVGGA has been applied to several solids and compared with other GGA-based calculations [2, 3, 23]. It has been concluded that EVGGA in general improves the band gap and some other properties which mainly depend on the accuracy of exchange–correlation potential, while for calculating the properties which are based on total energy calculations, such as the equilibrium lattice parameter and bulk modulus, usual GGAs are more appropriate. Hence, in the present work we first obtained the equilibrium lattice constant and optimized internal parameters by GGA96 and subsequently applied them to calculate the band structure of $Mg_{3x}Be_{3-3x}N_2$ ternary alloy along high symmetry directions in 1BZ by both EVGGA and GGA96. The band structure results are presented in table 5. The overall band structure behaviour for all compositions was found to be similar, therefore as a prototype the band structure curve for $x = 0.25$ is shown in figure 5. The deviation of band gap from the LCD prediction, with bowing parameter equal to

Table 5. The band gap, E_g, the valence bandwidth and the s–p gap (the energy gap between two parts of the valiance bands), E_{s-p}, calculated within GGA96 and EVGGA are compared with other theoretical and experimental available results.

			Valence bandwidth (eV)		
X	Method	E_g (eV)	Upper	Lower	E_{s-p} (eV)
0	DFT (GGA96)[a]	3.33	7.49	3.13	5.83
	DFT (EVGGA)[a]	4.17	7.18	2.95	6.39
	HF[b]	12.69	—	—	—
	HF + (DFT_correction)[b]	4.28	7.49	3.10	6.06
	Exp.[c]	3.8	—	—	—
1/4	DFT (GGA96)	2.89	6.40	3.00	5.94
	DFT (EVGGA)	3.65	6.09	2.83	6.47
1/3	DFT (GGA96)	2.65	6.17	2.54	6.19
	DFT (EVGGA)	3.35	5.99	2.38	6.69
2/4	DFT (GGA96)	2.38	5.63	2.31	6.38
	DFT (EVGGA)	3.17	5.27	2.15	7.01
2/3	DFT (GGA96)	1.98	4.99	1.81	6.95
	DFT (EVGGA)	2.71	4.23	1.63	7.69
3/4	DFT (GGA96)	1.86	4.88	1.70	7.15
	DFT (EVGGA)	2.59	4.16	1.62	7.97
1	DFT (GGA96)[a]	1.56	4.09	1.43	7.52
	DFT (EVGGA)[a]	2.22	3.77	1.30	8.07
	HF + (DFT_correction)[b]	2.25(Γ–N)	3.89	1.29	7.94

[a] Reference [3].
[b] Reference [5].
[c] Reference [24].

0.447 and 0.424 eV obtained by using EVGGA and GGA96 respectively, is plotted in figure 6. The main features to note from the band structure calculations are as follows:

(1) The occupied bands for all compositions are separated into two sub-bands with widths that are decreasing and a gap that is increasing with concentration of Mg.

(2) The value obtained for the direct band gap (Γ–Γ) between valence and conduction bands decreases with growing concentration of Mg. This behaviour can be explained as follows [25]. While in the process of increasing concentration the nuclear charge increase is exactly balanced by a similar increase in the core electron number, but the larger number of core electrons is more effective in screening the nuclear charge. Thus, the valence levels in Mg are less tightly bound compared to Be, and this is reflected in the more metallic character of the Mg_3N_2 band structure with respect to the α-Be_3N_2 compound. The same behaviour has been seen in the III-N compounds and their alloys [10].

(3) The band gap fluctuations around the polynomial fitted curve are larger than the corresponding values for the total energy parameters such as lattice constants, bulk modulus and cohesive energy. This is simply a result of the fact that the band gap is more sensitive to the details of the structure, while the total energy properties are average quantities obtained from integrals over the Brillouin zone and thus show fewer fluctuations. In general, good atomic relaxation and subsequent force convergency can reduce the band gap fluctuations. In our calculations, the mean value of the forces for each composition was decreased to less than 10 mRyd/au.

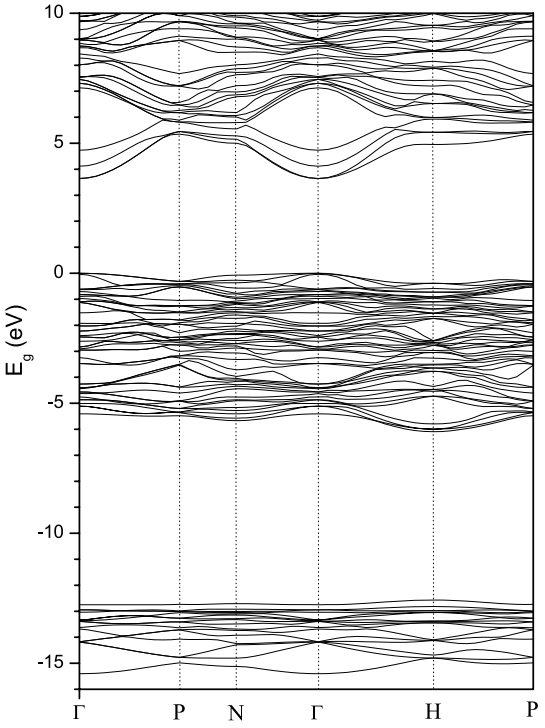

Figure 5. Band structure of $Mg_{3x}Be_{3-3x}N_2$ for $x = 0.25$ obtained by EVGGA at equilibrium lattice parameter. The direct band gap is about 3.65 eV at the Γ point.

(4) Although GGA96 and EVGGA predict different values for the band gap [3], the corresponding bowing parameters within these two approximations are rather close to each other. This result confirms the calculated band gap bowing.

Finally, the total (whole cell contribution) and partial (site-decomposed local) density of states (DOS) were calculated by the tetrahedral method [26] using EVGGA and GGA96 for $x = 0, \frac{1}{4}, \frac{1}{3}, \frac{2}{4}, \frac{2}{3}, \frac{3}{4}, 1$ in $Mg_{3x}Be_{3-3x}N_2$ alloy. The DOS curve for $x = 0.25$ is presented as a prototype in figure 7. The fundamental points to note from these calculations are as follows:

(1) The total density of states for all compositions is rather similar; the valence band is split into two sub-bands, a narrow sub-band located deep in the lower energy range and a wider one near to the Fermi level. The s orbitals of the four non-equivalent N atoms have the major contribution to the lower valence sub-band with a width that decreases by increasing x. This means that the electrons located in this band are more localized for lower beryllium molar fraction. The upper valence sub-band for all compounds is mainly dominated by the nitrogen 2p states, with a minor contribution from s and p orbitals of Be and Mg atoms.
(2) It is evident from this plot that the p orbitals of N atoms hybridize with the s and p states of Be and Mg atoms in the upper valence sub-band, while the s orbitals of N atoms do not have any overlapping with other orbitals.
(3) The conduction bands are mainly constructed by the s and p orbitals of metal atoms (Be, Mg) with the minimum occurring at the Γ point, and the contribution of p orbitals of N atoms is ignorable.

4. Conclusion

We have studied the electronic and structural properties of $Mg_{3x}Be_{3-3x}N_2$ ternary alloy by first-principles FP-LAPW calculations. To our knowledge no theoretical and experimental study has

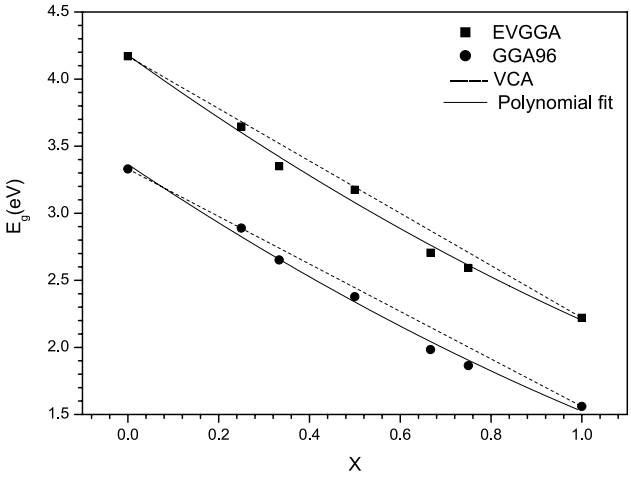

Figure 6. The composition dependence of the calculated band gap of $Mg_{3x}Be_{3-3x}N_2$ alloy compared with the LCD prediction (dashed line). The bowing parameters equal to 0.447 and 0.424 eV were obtained by using EVGGA and GGA96 respectively and fitting the data with a polynomial (solid curve).

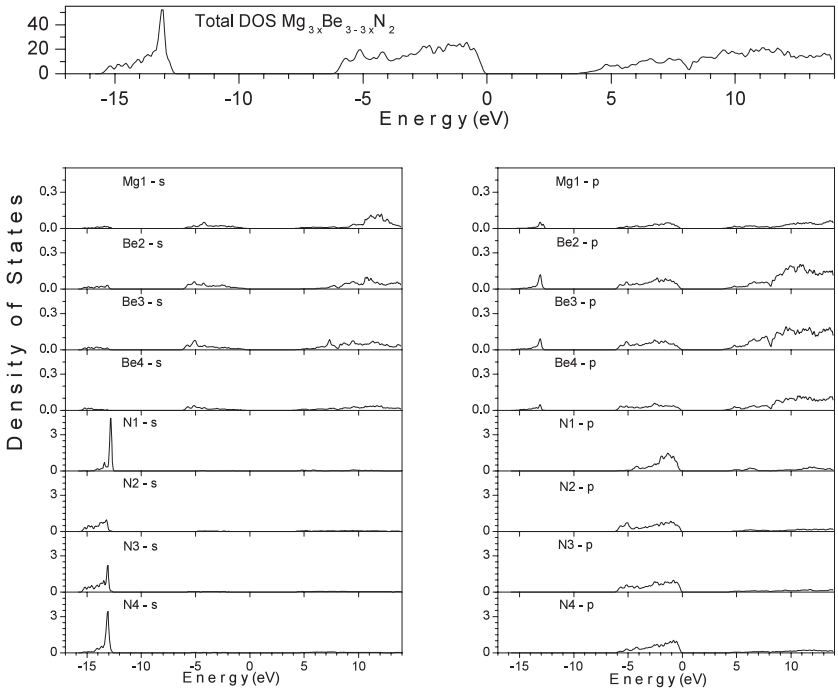

Figure 7. Total (DOS/eV/unit cell) and partial density of states (DOS/eV/atom) for contributions of the s and p atomic orbitals in $Mg_{3x}Be_{3-3x}N_2$ alloy for $x = 0.25$ using EVGGA.

been reported so far on the structural and electronic properties of this alloy, hence our results can serve as a prediction for future study. We focused in particular on the composition dependence of the electronic and structural parameters of this alloy. The values obtained for internal and structural parameters at $x = 0, 1$ are in good agreement with the available experimental and

theoretical results. Although the lattice parameters, bulk modulus and cohesive energy do not follow an LCD they can be explained by constant bowing parameters. We obtained an upward bowing parameter equal to -0.704 Å for the lattice constants, a downward bowing parameter with a value of 0.802 Mbar for the bulk modulus, and a downward bowing for the cohesive energy with a value of 0.9966 eV/atom. The source of these rather large deviations from LCD is probably due to the 10% lattice mismatch between α-Be_3N_2 and Mg_3N_2 binary compounds. In band structure calculations, we find out that although the electronic many body effects, as evaluated within GGA96 and EVGGA, significantly affect the absolute value of the band gaps they leave the bowing parameter nearly unaffected. A hybridization between p orbitals of N atoms and s and p states of Be and Mg atoms is concluded from DOS calculations for all compositions.

Acknowledgment

This work was financially supported by Isfahan University of Technology.

Appendix

M_3N_2 (M = Be, Mg) has 40 atoms per primitive cell, 24 similar M atoms and two types of N atoms, 4N1 and 12N2. The positions of the atoms in this structure are as follows [17]:

N1: $\frac{1}{4}, \frac{1}{4}, \frac{1}{4}; \frac{1}{4}, \frac{3}{4}, \frac{3}{4}; \frac{3}{4}, \frac{1}{4}, \frac{3}{4}; \frac{3}{4}, \frac{3}{4}, \frac{1}{4}$

N2: $\pm(u, 0, \frac{1}{4}; \frac{1}{4}, u, 0; 0, \frac{1}{4}, u; -u, \frac{1}{2}, \frac{1}{4}; \frac{1}{4}, -u, \frac{1}{2}; \frac{1}{2}, \frac{1}{4}, -u)$

M: $\pm(x, y, z; x, -y, \frac{1}{2} - z; \frac{1}{2} - x, y, -z; -x, \frac{1}{2} - y, z)$

$\pm(z, x, y; \frac{1}{2} - z, x, -y; -z, \frac{1}{2} - x, y; z, -x, \frac{1}{2} - y)$

$\pm(y, z, x; -y, \frac{1}{2} - z, x; y, -z, \frac{1}{2} - x; \frac{1}{2} - y, z, -x).$

The atomic positions of $Mg_{3x}Be_{3-3x}N_2$ alloy for $x = \frac{1}{3}, \frac{2}{3}$ are as follows:

N1: $\frac{1}{4}, \frac{1}{4}, \frac{1}{4}; \frac{1}{4}, \frac{3}{4}, \frac{3}{4}; \frac{3}{4}, \frac{1}{4}, \frac{3}{4}; \frac{3}{4}, \frac{3}{4}, \frac{1}{4}$

N2: $\pm(u_2, 0, \frac{1}{4}; -u_2, \frac{1}{2}, \frac{1}{4})$

N3: $\pm(\frac{1}{4}, u_3, 0; \frac{1}{4}, -u_3, \frac{1}{2})$

N4: $\pm(0, \frac{1}{4}, u_4; \frac{1}{2}, \frac{1}{4}, -u_4)$

$x = \frac{1}{3}$:

Mg1 $\pm$ $(x_1, y_1, z_1; x_1, -y_1, \frac{1}{2} - z_1; \frac{1}{2} - x_1, y_1, -z_1; -x_1, \frac{1}{2} - y_1, z_1)$

Be2 $\pm$ $(z_2, x_2, y_2; \frac{1}{2} - z_2, x_2, -y_2; -z_2, \frac{1}{2} - x_2, y_2; z_2, -x_2, \frac{1}{2} - y_2)$

Be3 $\pm$ $(y_3, z_3, x_3; -y_3, \frac{1}{2} - z_3, x_3; y_3, -z_3, \frac{1}{2} - x_3; \frac{1}{2} - y_3, z_3, -x_3)$

$x = \frac{2}{3}$:

Mg1 $\pm$ $(x_1, y_1, z_1; x_1, -y_1, \frac{1}{2} - z_1; \frac{1}{2} - x_1, y_1, -z_1; -x_1, \frac{1}{2} - y_1, z_1)$

Mg2 $\pm$ $(z_2, x_2, y_2; \frac{1}{2} - z_2, x_2, -y_2; -z_2, \frac{1}{2} - x_2, y_2; z_2, -x_2, \frac{1}{2} - y_2)$

Be3 $\pm$ $(y_3, z_3, x_3; -y_3, \frac{1}{2} - z_3, x_3; y_3, -z_3, \frac{1}{2} - x_3; \frac{1}{2} - y_3, z_3, -x_3).$

The atomic positions of $Mg_{3x}Be_{3-3x}N_2$ alloy for $x = \frac{1}{4}, \frac{2}{4}, \frac{3}{4}$ are as follows:

N1: $\frac{1}{4}, \frac{1}{4}, \frac{1}{4}$

N2: $\frac{1}{4}, \frac{3}{4}, \frac{3}{4}; \frac{3}{4}, \frac{1}{4}, \frac{3}{4}; \frac{3}{4}, \frac{3}{4}, \frac{1}{4}$

N3: $\pm(v_1, v_2, v_3; v_3, v_1, v_2; v_2, v_3, v_1)$

N4: $\pm(v_1', v_2', v_3'; v_3', v_1', v_2'; v_2', v_3', v_1')$

$x = \frac{1}{4}$:

Mg1 $\pm (x_1, y_1, z_1; z_1, x_1, y_1; y_1, z_1, x_1)$

Be2 $\pm (x_2, -y_2, \frac{1}{2} - z_2; \frac{1}{2} - z_2, x_2, -y_2; -y_2, \frac{1}{2} - z_2, x_2)$

Be3 $\pm (\frac{1}{2} - x_3, y_3, -z_3; -z_3, \frac{1}{2} - x_3, y_3; y_3, -z_3, \frac{1}{2} - x_3)$

Be4 $\pm (-x_4, \frac{1}{2} - y_4, z_4; z_4, -x_4, \frac{1}{2} - y_4; \frac{1}{2} - y_4, z_4, -x_4)$

$x = \frac{2}{4}$:

Mg1 $\pm (x_1, y_1, z_1; z_1, x_1, y_1; y_1, z_1, x_1)$

Mg2 $\pm (x_2, -y_2, \frac{1}{2} - z_2; \frac{1}{2} - z_2, x_2, -y_2; -y_2, \frac{1}{2} - z_2, x_2)$

Be3 $\pm (\frac{1}{2} - x_3, y_3, -z_3; -z_3, \frac{1}{2} - x_3, y_3; y_3, -z_3, \frac{1}{2} - x_3)$

Be4 $\pm (-x_4, \frac{1}{2} - y_4, z_4; z_4, -x_4, \frac{1}{2} - y_4; \frac{1}{2} - y_4, z_4, -x_4)$

$x = \frac{3}{4}$:

Mg1 $\pm (x_1, y_1, z_1; z_1, x_1, y_1; y_1, z_1, x_1)$

Mg2 $\pm (x_2, -y_2, \frac{1}{2} - z_2; \frac{1}{2} - z_2, x_2, -y_2; -y_2, \frac{1}{2} - z_2, x_2)$

Mg3 $\pm (\frac{1}{2} - x_3, y_3, -z_3; -z_3, \frac{1}{2} - x_3, y_3; y_3, -z_3, \frac{1}{2} - x_3)$

Be4 $\pm (-x_4, \frac{1}{2} - y_4, z_4; z_4, -x_4, \frac{1}{2} - y_4; \frac{1}{2} - y_4, z_4, -x_4)$.

References

[1] Vurgaftman I and Meyer J R 2003 *J. Appl. Phys.* **94** 3675
[2] Mokhtari A and Akbarzadeh H 2002 *Physica* B **324** 305
[3] Mokhtari A and Akbarzadeh H 2003 *Physica* B **337** 122
[4] Lambrecht W R L and Segall B 1992 *Phys. Rev.* B **45** 1485
[5] Armenta M G M, Reyes-Serrato A and Borja M A 2000 *Phys. Rev.* B **62** 4890
[6] Armenta M G M and Reyes-Serrato A 2001 *Comput. Mater. Sci.* **21** 95
[7] Heyns A M and Prinsloo L C 1998 *J. Solid State Chem.* **137** 33
[8] Reyes-Serrato A, Soto G, Gamietea A and Farias M H 1998 *J. Phys. Chem. Solids* **59** 743
[9] Sökeland F, Rohlfing M, Krüger P and Pollmann J 2003 *Phys. Rev.* B **68** 75203
[10] Dridi Z, Bouhafs B and Ruterana P 2003 *Semicond. Sci. Technol.* **18** 850
[11] Wu J, Walukiewicz W, Yu K M, Ager J W III, Haller E E, Lu H and Schaff W J 2002 *Appl. Phys. Lett.* **80** 4741
[12] Blaha P, Schwarz K, Madsen G K H, Kvasnicka D and Luitz J 2001 *WIEN2k, An Augmented Plane Wave+Local Orbitals Program for Calculating Crystal Properties* ed K Schwarz (Austria: Techn. Universität Wien) ISBN 3-9501031-1-2
[13] Hohenberg P and Kohn W 1964 *Phys. Rev.* **136** B864
[14] Kohn W and Sham L J 1965 *Phys. Rev.* **140** A1133
[15] Perdew J P, Burke K and Ernzerhof M 1996 *Phys. Rev. Lett.* **77** 3865
[16] Engel E and Vosko S H 1993 *Phys. Rev.* B **47** 13164
[17] Wyckoff R W G 1986 *Crystal Structures* 2nd edn (Malabar, FL: Krieger)
[18] Murnaghan F D 1944 *Proc. Natl Acad. Sci. USA* **30** 244
[19] Ferhat M and Bechstedt F 2002 *Phys. Rev.* B **65** 75213
[20] Cohen M L 1985 *Phys. Rev.* B **32** 7988
[21] Tsai M H, Peiris F C, Lee S and Furdyna K 2002 *Phys. Rev.* B **65** 235202
[22] Martins J L and Zunger A 1986 *Phys. Rev. Lett.* **56** 1400
[23] Dufek P, Blaha P and Schwarz K 1994 *Phys. Rev.* B **50** 7279
[24] Soto G, Díaz J A, Machorro R, Reyes-Serrato A and de la Cruz W 2002 *Mater. Lett.* **52** 29
[25] Cohen M L and Chelikowsky J R 1988 *Electronic Structure and Optical Properties of Semiconductors* (Berlin: Springer)
[26] Blöchl P E, Jepsen O and Andersen O K 1994 *Phys. Rev.* B **49** 16223